AD-772 634

CORRELATION OF MICRO- AND MACRO-
SCOPIC STRUCTURES OF WIND WAVES AND
DIFFERENTIAL ROUGHENING AND SMOOTHING
OF SURFACE WAVES BY WIND

Jin Wu

Hydronautics, Incorporated

AD 772 634

HYDRONAUTICS, Incorporated
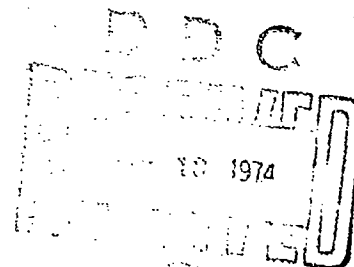
ib

CORRELATION OF MICRO- AND
MACROSCOPIC STRUCTURES OF
WIND WAVES AND DIFFERENTIAL
ROUGHENING AND SMOOTHING OF
SURFACE WAVES BY WIND

By

Jin Wu

November 1973

D D C

IC 1974

The views and conclusions contained in this document
are those of the author's and should not be interpreted
as necessarily representing the official policies,
either expressed or implied, of the Advanced Research
Projects Agency or the U. S. Government

SECURITY CLASSIFICATION OF THIS PAGE (When Data Entered)

AD 772634

REPORT DOCUMENTATION PAGE		READ INSTRUCTIONS BEFORE COMPLETING FORM
1. REPORT NUMBER T. R. 7211-6	2. GOVT ACCESSION NO.	3. RECIPIENT'S CATALOG NUMBER
4. TITLE (and Subtitle) CORRELATION OF MICRO- AND MACROSCOPIC STRUCTURES OF WIND WAVES AND DIFFERENTIAL ROUGHENING AND SMOOTHING OF SURFACE WAVES BY WIND		5. TYPE OF REPORT & PERIOD COVERED Technical Report
		6. PERFORMING ORG. REPORT NUMBER T. R. 7211-6
7. AUTHOR(s) Jin Wu		8. CONTRACT OR GRANT NUMBER(s) N00014-72-C-0509
9. PERFORMING ORGANIZATION NAME AND ADDRESS HYDRONAUTICS, Incorporated 7210 Pindell School Rd, Howard County, Laurel, Md. 20810		10. PROGRAM ELEMENT, PROJECT, TASK AREA & WORK UNIT NUMBERS NR 062-472
11. CONTROLLING OFFICE NAME AND ADDRESS Advanced Research Projects Agency Arlington, Va. 22209		12. REPORT DATE November 1973
		13. NUMBER OF PAGES 36
14. MONITORING AGENCY NAME & ADDRESS(if different from Controlling Office) Office of Naval Research Department of Defense Arlington, Va. 22209		15. SECURITY CLASS. (of this report) UNCLASSIFIED
		15a. DECLASSIFICATION/DOWNGRADING SCHEDULE

16. DISTRIBUTION STATEMENT (of this Report)

This document has been approved for public release and sale;
its distribution is unlimited.

17. DISTRIBUTION STATEMENT (of the abstract entered in Block 20, if different from Report)

18. SUPPLEMENTARY NOTES

19. KEY WORDS (Continue on reverse side if necessary and identify by block number)

Wind Waves
Microstructure of Sea Surface
Roughness of Sea Surface
Wind-Wave Interaction

Wave-Wave Interaction

20. ABSTRACT (Continue on reverse side if necessary and identify by block number)

Simultaneous measurements were conducted in a wind-wave tank of the ripple slopes with an optical instrument and of the carrier-wave profiles with a wave-height gage. The experiments were conducted under various wind conditions: either steady or unsteady wind blowing over pre-existing regular surface waves. The data were analyzed to determine the slope distributions of ripples

20. (Continued)

located on various portions of the carrier-wave profiles under
steady wind, and the differential roughening and smoothing of the
carrier waves under unsteady wind. The influences of pre-existing
waves on the structure of the wind boundary layer, and on the
slope statistics of ripples were also studied.

HYDRONAUTICS, Incorporated

TABLE OF CONTENTS

HYDRONAUTICS, Incorporated

LIST OF FIGURES

HYDRONAUTICS, Incorporated

ABSTRACT

Simultaneous measurements were conducted in a wind-wave tank of the ripple slopes with an optical instrument and of the carrier-wave profiles with a wave-height gage. The experiments were conducted under various wind conditions: either steady or unsteady wind blowing over pre-existing regular surface waves. The data were analyzed to determine the slope distributions of ripples located on various portions of the carrier-wave profiles under steady wind, and the differential roughening and smoothing of the carrier waves under unsteady wind. The influences of pre-existing waves on the structure of the wind boundary layer, and on the slope statistics of ripples were also studied.

1. INTRODUCTION

The wind-disturbed water surface features ripples riding on long waves. There has been a great deal of interest in determining the statistical description of the microstructure of the disturbed surface, the pattern of ripples. These wavelets were considered (Phillips 1966) to be involved in the inception of wind waves as well as in the dissipation of wave energy. In addition, the microstructure was also suggested to govern the reflection and the backscattering of the electromagnetic waves (Newton and Rouse 1972) impinging on, and the radiation of thermal energy (McGrath and Osborne 1973) from, the air-sea interface.

Some measurements (Schooley 1954, Cox and Munk 1956, Cox 1958, Wu 1971a, 1972a) have been conducted in the past to determine the slope and curvature distributions of wind waves under various wind velocities. There is, however, a lack of detailed studies of the distributions of ripples along the profiles of the carrier waves and the correlations of these distributions with wind and wave conditions. Such distributions are helpful for understanding energy transfer processes from wind to waves (Longuet-Higgins 1969, Wu 1972b), and between wave components (Longuet-Higgins 1963, Phillips 1963). These distributions are also helpful for setting the viewing angle of the microwave sensor over the sea surface and interpreting results of microwave measurements. It should also be pointed out that all the past measurements of ripples were conducted under steady winds. Yet the roughening of the water surface by a suddenly started wind, and the dissipation of ripple energy following a suddenly stopped wind, should be more revealing of the mechanism of dynamic interaction between wind and waves, or even among wave components. This kind of measurement of the microstructure under unsteady wind is also desirable for modeling the air-sea interface, because the natural wind is generally unsteady.

In the present study, the carrier-wave profiles and the ripple slopes were simultaneously measured at a fixed point in a laboratory wind-wave tank under various wind velocities. For the convenience of experiments conducted under a short fetch, pre-existing regular surface waves were generated. Each series of

experiments included three phases with the following sequence of wind and wave conditions; a suddenly started wind over a calm water surface, a steady wind over an equilibrium disturbed water surface, and a suddenly stopped wind over an initially disturbed surface. Features of the correlations between the micro-and macroscopic structures of the disturbed water surface under steady winds, and patterns of the differential roughening and decay of the microstructure under unsteady winds, are herein presented.

2. EXPERIMENTAL CONDITIONS AND PROCEDURES

2.1 Equipment

The experiments have been conducted in a wind-wave tank, which is 1.5 m wide and 22 m long. Mounted at the upwind end of the tank is an axial-flow fan, driven by a variable-speed motor; a permeable wave absorber is installed at the downwind end. The tank is covered for the first 15 m to provide a 0 31-m high wind tunnel above 1.24-m deep water. The maximum obtainable wind velocity within the tunnel is 14 m/s. The test section is located at the middle length of the tank.

The tank is also equipped with a mechanical wave generator, a flap with its lower edge hinged at the bottom of the tank and with its upper edge oscillated at any desired frequency and amplitude by a motor. The fan and the mechanical wave generator can be operated either separately or simultaneously.

2. Wind and Wind Measurements

The differential roughening and smoothing of the regular waves were studied with a suddenly started and a suddenly stopped wind, respectively. The instantaneous starting or stopping of the wind was achieved by means of a curtain supported at the air intake of the fan. The curtain can be either rolled up around a metal pipe attached at its lower edge, or hung in front of the intake. When the fan turns, the curtain is sucked against the heavy-wire grid at the intake to block completely the airflow. For measurements of wave decay, the curtain is up initially while the wind blows steadily to build up an equilibrium microstructure in the tank. Subsequently, the fan is turned off and at the same time the metal pipe is released to drop the curtain. For measurements of wave growth, the curtain is down while the fan is turned on to build up the required speed. Subsequently, the curtain is suddenly rolled up around the metal pipe. It was determined that one second was required to cover completely the fan section and one and one-half seconds was necessary to open it up completely. Such an arrangement with the curtain is needed, because the mechanical inertia of the fan makes it impossible to either start or stop the airflow suddenly. Following the lift or drop of the curtain, the energy supplied by the wind was either suddenly present or completely cut off, and the microstructure in the tank varied rapidly.

The velocity distributions of steady winds blowing over pre-existing waves were determined with a pitot-static probe and a differential pressure transducer unit. The probe was supported

successively at various elevations above the water surface. The
output of the pressure transducer, which is proportional to the
square of the velocity, was first fed to a square-root circuitry
and then displayed on an x-y plotter. At each elevation, the ve-
locity was continuously recorded for a period of 30 seconds. The
latter is much longer than the period of surface waves, and the
average wind velocity at each elevation can be determined.

2.3 Waves and Wave Measurements

Two types of instruments have been used simultaneously in
this experiment: a conductivity probe for recording carrier-wave
profiles and an optical instrument for measuring ripple slopes.
The conductivity probe consists primarily of a partially sub-
merged platinum wire, supported vertically at the test section.
The output of the electric current flowing through the probe is
proportional to the submergence of the wire. The probe, however,
does not provide enough resolution for measuring wavelets that
ride on top of long waves and have amplitudes only a fraction of
the latter.

The optical instrument consists principally of a light source
and a telescope and photomultiplier unit. Supported over the wind-
wave tank, the instrument can be set at any desired inclination
from the water surface. The photomultiplier receives reflected
light only when the water surface is normal to the plane contain-
ing the light sheet and the telescopic axis. The cross sections
of the light sheet is rectangular with a large length-to-width

ratio and with its short side aligned with the direction of the
wind. The instrument is, therefore, insensitive to the crosswind
slope; the angular tolerance of the instrument to the water sur-
face slope is about 1° in the longitudinal (wind) direction and
is about 20° in the transverse direction. During the experiment,
the instrument was set successively at various inclinations to
measure the frequencies of occurrence of the corresponding upwind-
downwind slopes of the disturbed surface. A detailed description
of the instrument has been reported earlier (Wu 1971a).

For the major portion of the measurements, the outputs of
the wave-height gage and of the optical instrument were recorded
simultaneously on different channels of a tape recorder. Details
of these measurements and data processing — correlation between
micro-and macroscopic structures, growth and decay of ripples
over carrier waves — will be discussed in later sections.

Since the wind-induced drift is known (Phillips 1973a, Wu
1973a) to modify the propagation of surface waves, additional
experiments were conducted to measure the carrier waves under
various wind velocities. As the wind blew harder, the carrier
waves became more and more sharply peaked, but remained regular.
Two wave probes were used during this part of the experiment:
the upwind probe was fixed and the downwind probe was supported
on a sliding scale. The distance between probes was adjusted to
make the wave signals from two probes, monitored on the scope,
oscillating in phase. This distance is therefore the wavelength.
The heights and lengths of carrier waves under various wind ve-
locities are shown in Figure 1. On the other hand, the wave

HYDRONAUTICS, Incorporated

height is seen to increase slowly at low wind velocities, more
effectively at medium wind velocities, and again slowly at high
wind velocities where violent wave breaking occurs. The varia-
tion of the wavelength with the wind velocity appears to be
consistent with that of the wave height; where the wave height
increases more effectively with the wind velocity, the wavelength
increases less effectively.

2.4 Correlation Measurements

The signals of the photomultiplier produced by the wind-
disturbed water surface are light pulses having various intensities
and various durations. The intensity is related to the surface
curvature (Wu 1972a) and the duration is the period for transfer-
ring under the instrument a slope within the slope-tolerance limit
(1°) of the optical instrument. The period and the intensity of
the pulse were not measured here, and each signal was reshaped as
a pulse of a constant duration and intensity. Each shaped pulse,
therefore, represents the occurrence of a given slope of the water
surface regardless of its transferring speed and its curvature.

For the correlation measurements under steady wind, the
carrier-wave profile was divided into four regions: upper and
lower halves of either the windward or the leeward face. A gating
device was designed for partitioning and collecting the light
signals from each region. During the operation, the tape was
played back at one quarter of the recording speed with the carrier-
wave profile monitored on the oscilloscope and with the pulse
signal passing through the gating device. The latter was controlled

by an operator who watched the slow varying carrier waves shown
on the scope. The gating device was operated so as to feed only
the light pulses from the desirable portion of the carrier-wave
profile to the pulse analyzer. The tape was repeatedly run to
obtain successively the data for the following portions of the
carrier-wave profile: (1) the leeward face, (2) the upper half
of the leeward face, and (3) the upper half of the windward face.
On the basis of these three sets of data, in addition to the
data obtained from the entire carrier-wave profile, the results
for all four regions mentioned earlier can be deduced.

2.5 Growth and Decay Measurements

When the tape was played back, the number of pulses was also
accumulated on a counter. Under a steady wind, the accumulation
of the equilibrium-state data could be started at an arbitrary
point of the tape. For the wave growth and decay data, the ac-
cumulation was started immediately following the identification
signal indicating the instant when the wind was either suddenly
started or completely stopped. The number of pulses accumulated
on the counter was sampled by a printer. The sampling rate can
be varied, with the maximum rate at eight numbers per second.
The printout is, therefore, the temporal accumulation of the fre-
quency of occurrence of a given water-surface slope following the
change of wind conditions. For each wind velocity this process
was repeated for various water-surface slopes.

HYDRONAUTICS, Incorporated

-9-

3. WIND BOUNDARY LAYER OVER PRE-EXISTING WAVES

3.1 Wind-Velocity Profiles

The wind velocity profiles in the tunnel over the pre-existing regular waves are plotted in Figure 2a, b, where u is the wind velocity measured at the distance y above the mean water surface. Two series of velocity surveys were performed with pre-existing regular waves of the same frequency but different amplitudes. Series (a) with larger wave amplitudes is the primary series under which the experiments on correlation, and differential roughening and smoothing were conducted; series (b) is the secondary series, which was performed only to study effects of pre-existing waves on the wind boundary layer.

The wind velocity is seen in Figure 2 to follow the logarithmic law (Schlichting 1968, Chapter XIX), or to vary linearly with the logarithm of the distance above the water surface. The wave-induced air motion, however, is considerable near the water surface where the data are greatly scattered. This portion of the data, generally having a smaller gradient, is omitted from Figure 2. The distorted region appears to extend further away from the water surface for waves of larger amplitudes. This is not only illustrated by the data obtained under various wind velocities shown separately in Figure a, b, but also from the comparison of the logarithmic profile shown in Figure 2b with that for the corresponding wind velocity shown in Figure 2a.

HYDRONAUTICS, Incorporated

3.2 Effects of Pre-Existing Waves on Wind Boundary Layer

The shear velocity (u_*) of the wind and the roughness length
(k) of the disturbed water surface, calculated from the velocity
profile shown in Figure 2, are plotted in Figure 3a, b. The wind
velocity U shown in Figure 3 is that measured at 2/3 of the tun-
nel height above the mean water surface. The solid lines shown
in the figure indicate the results obtained at the same test sec-
tion with wind blowing over initially calm water surface (Wu
1973b). The effects of pre-existing waves on wind boundary layer
are better illustrated through the results of the roughness length
than those of the shear velocity; see Figure 3a, b. The roughness
length, which is related to the intercept of the wind profile, is
more sensitive to a small change of the velocity gradient than the
shear velocity, which are related to the slope of the profile.

Similar to earlier results with wind blowing over initially
calm water surface, the data of shear velocity and roughness
length obtained here with pre-existing waves are divided into two
groups according to whether wind-wave interaction is governed by
surface tension or gravity. The shear velocity increases gradually
with the wind velocity in the former regime, and rapidly in the
latter regime. The roughness length decreases with the wind ve-
locity in the former regime, and increases with the wind velocity
in the latter regime. Physically, these two regimes correspond
respectively, to the presence of parasitic capillaries, and to
the occurrence of airflow separation and wave breaking. Without
pre-existing waves, the dividing velocity of these two regimes is

HYDRONAUTICS, Incorporated

about 9 m/s. With pre-existing waves, this velocity is lowered
to 7 m/s, at which wave breaking starts. In other words, the
pre-existing waves concentrate the energy transfer from wind to
waves of a particular length and therefore promote wave breaking
at its crest.

At low wind velocities in the surface-tension governing
regime of wind-wave interaction, the pre-existing waves are seen
in Figure 3b to smooth the water surface hydrodynamically. With
pre-existing waves, the carrier waves of parasitic capillaries
are much longer. Consequently, the number of capillaries per
unit area of the water surface is greatly reduced. Therefore,
inasmuch as the capillaries govern the dissipation of wave energy,
the water surface becomes smoother with long pre-existing waves.
The surface with large-amplitude, pre-existing waves is seen in
Figure 3b to be hydrodynamically smoother than that with small-
amplitude pre-existing waves. Because the regularity of carrier
waves in the latter case was somewhat disrupted by the wind, short
gravity waves with parasitic capillaries were observed superim-
posing on long carrier waves.

At high wind velocities in the gravity governing regime of
wind-wave interaction, the airflow separation from wind waves
occurs in the present tank (Wu 1968). In this case, with the wind
blowing over initially calm water, the roughness length was found
to be comparable to the wave height. The separation pocket is
likely to cover a major portion of the windward face of the next
wave. With pre-existing waves, the peak of carrier waves is again

sharply cusped, and the airflow separation from the peak should
again occur. However, the separation pocket near the cusped peak,
although larger in volume than that taking place without pre-
existing waves, can hardly reach the windward face of the next
wave. In other words, with pre-existing waves, the separation
pockets are likely to be further isolated, and the density of
roughness element is therefore reduced. Since the aerodynamic
roughness depends on both the height and the density of the rough-
ness elements (Schlichting 1968, Chapter XX), the more widely
spaced separation pockets due to pre-existing waves cause a re-
duction of the roughness length. Consequently, the roughness
length with pre-existing waves is smaller than the wave height.
Very little difference of the roughness length is seen in Fig-
ure 3b between two cases with pre-existing waves of the same fre-
quency (length) but different amplitudes, because for these two
cases the roughness length is probably governed more by the
spacing than by the height of the roughness elements.

4. CORRELATION OF MICRO- AND MACROSCOPIC STRUCTURES OF WIND WAVES

The present experiment was conducted with wind waves super-
imposed on pre-existing regular surface waves. The use of me-
chanically generated waves is necessary not only for the study of
differential roughening and smoothing to be discussed in the next
section, but also for the correlation study. Otherwise it would
be very tedious to apply the gating technique to high-frequency,
irregular carrier waves. With wind blowing over pre-existing

HYDRONAUTICS, Incorporated

low-frequency waves, on the other hand, the carrier waves remain
regular and the undulation of the water surface can be more easily
traced by the operator. In other words, the pre-existing waves
also serve as the regulator for the present correlation measure-
ments.

4.1 Slope Distributions

The data obtained directly from the tape include the slope
distributions of ripples riding on the tops of the following por-
tions of the carrier-wave profile: (a) entire profile, (b) leeward
face, (c) upper half of leeward face, and (d) upper half of wind-
ward face. From these data, the slope distribution for ripples
riding on the top of the other portions of the carrier-wave pro-
files can be deduced: (a) windward face, (b) lower half of wind-
ward face, and (c) lower half of leeward face. The results for
four different wind velocities are shown in Figure 4, one column
for each wind velocity. Each row in Figure 4 indicates the data
obtained from the same portion of the carrier-wave profile. The
positive angle shown in the figure corresponds to a leeward slope,
and the negative angle corresponds to a windward slope. The data
shown in Figure 4 were obtained from a one-minute run of the ex-
periment. A smooth curve was fitted by eye to each set of data to
indicate a faired slope distribution.

The maximum frequency of occurrence of water-surface slope
should be produced by the peak and the trough of ripples. Since
they are tilted by the carrier waves, the peaks and troughs of
ripples do not have zero slopes. Consequently, the slope dis-
tribution for ripples riding on the leeward face of carrier waves

is peaked at a positive angle, and that for ripples riding on
the windward face is peaked at a negative angle. This trend is
clearly illustrated by the results shown in Figure 4. At low
wind velocities (U = 4.18, 6.92 m/s), the peakedness of the slope
distribution for the leeward face is much stronger than that for
windward face due to the presence of parasitic capillaries on the
leeward face. Such a difference disappears at high wind veloci-
ties, where ripples distributed more venly over the leeward and
the windward faces of carrier waves.

4.2 Effects of Pre-Existing Waves on Mean-Square Surface Slope

The mean-square slopes of the disturbed water surface with
pre-existing waves were determined from the slope distributions
shown on the top row of Figure 4. The results are tabulated in
Table 1.

TABLE 1

Mean-Square Slopes Measured with and
without Pre-Existing Waves

Wind Velocity, U (m/s)			4.18	6.92	9.60	10.25
Shear Velocity, u_* (m/s)			0.223	0.298	0.683	1.05
Mean-Square Surface Slope	With	Pre-existing Waves	0.0179	0.0219	0.0434	0.0527
	Without		0.0248	0.0426	0.0734	0.0021

HYDRONAUTICS, Incorporated

The shear velocity shown in Table 1 is the faired value obtained
from Figure 3a. The mean-square slopes of the disturbed water
surface without pre-existing waves were measured earlier (Wu
1972a, 1973c), and were related to the shear velocity of the
wind. The bottom row of Table 1 was obtained from earlier re-
sults.

For the same wind-shear velocity, mean-square slope with
pre-existing waves is seen in Table 1 to be smaller than that
without. This is 'n line with the earlier discussion concerning
the roughness length. With long pre-existing waves, the patches
of parasitic capillaries and the zones of wave breaking are more
widely spaced. Consequently, the density of roughness elements,
o.' number of ripples per unit area of the water surface, is re-
duced. In addition, there appears to be a spectral gap with
ripples superimposing long carrier waves, as waves of intermediate
lengths are missing. The mean-square slope of the water surface
is therefore reduced, since the roughness elements and short
carrier waves are the major contributor of the mean-square slope.

Even compared on the basis of wind-shear velocities, the up-
wind-downwind component of the mean-square water-surface slopes
measured in laboratory tanks were shown (Wu 1971a) to be smaller
than the oceanic results. This discrepancy was considered earlier
to be due in part, to the narrowness of the tank limiting the de-
velopment of the crosswind component of the mean-square slope.
The present results apparently suggest another contributing factor

HYDRONAUTICS, Incorporated

-16-

of this still not fully explained discrepancy. The long carrier
waves in the open ocean may cause the reduction of mean-square
slopes.

4.3 Distribution of Ripples along Carrier-Wave Profiles

As discussed in the previous section, the maximum frequency
of occurrence of the water-surface slope, or the peak of the
slope-distribution curve, appears to correspond to twice the num-
ber of ripples. Composite pictures showing the distributions of
ripples on various segments of carrier-wave profiles at different
wind velocities are presented in Figure 5. The four numbers in-
dicated along the wave profile are the relative frequencies of
occurrence of ripples riding on four respective segments of the
carrier-wave profile, the numbers on top of the profile are the
relative frequencies for the windward and the leeward faces, and
the numbers on the right side are those for the upper and the
lower half of the profile. At high wind velocities (U = 9.60,
12.5 m/s) the carrier-wave profile becomes skewed with shorter
leeward face and longer windward face. The numbers in parentheses
are the weighted values taking the skewness of the carrier-wave
profile into consideration.

On the basis of these composite pictures, the distribution
of surface roughnesses appear to have the following features:

(a) At low wind velocities (U = 4.18, 6.92 m/s) of
the surface-tension governing regime of wind-wave
interaction, the leeward face of the carrier wave
is much rougher than the windward face due to the
presence of parasitic capillaries.

(b) At high wind velocities (U = 9.60, 12.25 m/s) of
gravity-governing regime of wind-wave interaction,
the general trend is that as the wind velocity in-
creases the overall difference on roughening be-
tween leeward and the windward faces becomes less.

(c) In the surface-tension governing regime of wind-
wave interaction at two low wind velocities, the
parasitic capillaries are concentrated near the
upper half of the leeward face at U = 4.18 m/s,
and move further down the leeward face at U = 6.92
m/s.

(d) The breaking of wind waves (without pre-existing
mechanically generated surface waves) was observed
earlier (Wu 1971b) to occur on the leeward face
but very close to the wave peak. Excessive rough-
ness should therefore be concentrated on the upper
half of the leeward face of the carrier-wave pro-
file. With pre-existing waves, however, the rela-
tive frequency of occurrence of ripples on the
upper half of the windward face at U = 9.60 and
12.25 m/s is seen in Figure 5 to be greater than
that on the windward face. This is somewhat
surprising observations. It is worth noting that
the bubbling of the water surface and the three-
dimensional type roughness accompanying wave
breaking may escape the optical counting technique,
but not the glitter photography (Wu 1971b).

HYDRONAUTICS, Incorporated

(e) The lower half of the windward face is the smoothest segment of the carrier-wave profile.

5. DIFFERENTIAL ROUGHENING AND SMOOTHING OF A WAVY SURFACE

For a steady wind, the frequency of occurrence of a given water-surface slope (that is, the rate of light pulses detected by the optical instrument at a given angle of inclination) for an equilibrium, random wind-disturbed water surface should be nearly constant, $\bar{r}$. The equilibrium-state data were discussed in the previous section, and the distributions of $\bar{r}$ obtained from various segments of the carrier-wave profiles and under different wind velocities are presented in Figure 4.

In order to study the differential roughening of a wavy surface by wind and the differential decay of wind-excited ripples on a wavy surface, suddenly started and suddenly stopped winds were introduced. The frequencies of occurrence of water-surface slopes were determined with the optical instrument both during the growth stage (r_g) following a suddenly started wind, and during the decay stage (r_d) following a suddenly stopped wind. Applying the same procedure as that used earlier for the steady-state data, the growth and decay data were first obtained from certain portions of the carrier-wave profile, and subsequently, the results for the other portions of the profile were deduced. The data for the growth stage were obtained from a period of one minute, and those for the decay stage were obtained from a period

HYDRONAUTICS, Incorporated

of 30 seconds. The sampling interval of the printer is one
second for the growth stage and is one-half of one second for
the decay stage.

5.1 Growth and Decay of Root-Mean-Square Slopes

The values r_g and r_d are the frequencies of occurrence of
a particular water-surface slope at a given instant following,
respectively. the sudden starting and the sudden stopping of the
wind. At any given instant, the distribution of the water-sur-
face slopes can be obtained by compiling the instantaneous fre-
quencies of occurrence of various slopes. The temporal varia-
tions of the slope-distribution curves for the growth and the
decay stages, not shown here. follow a general pattern: namely,
widening with time for the growth stage and peaking with time
for the decay stage. Details of data analysis and of temporal
slope distributions are similar to those reported earlier (Wu
1973c) with wind blowing over initially calm water.

The variances of the water-surface slopes for ripples riding
on various portions of the carrier-wave profiles at various times
during the growth and the decay stages were calculated from the
instantaneous slope distributions. Subsequently, the variances
were normalized with respect to the value obtained from the en-
tire profile of carrier waves under steady wind. The temporal
variations of the normalized variances following the sudden start
and the sudden stop of the wind are plotted as light lines in
Figures 6 and 7, respectively. The horizontal axis in both fig-
ures indicates the time t after either the sudden start or the

HYDRONAUTICS, Incorporated

sudden stop of the wind. Generally, the data illustrates an exponential growth and an exponential decay of the water-surface slopes with time.

Two exponential curves of the following forms were fitted on the basis of the least-squares principles to the wave growth and decay data, respectively:

$$(\overline{s_g^2})^{\frac{1}{2}} \Big/ (\overline{s_o^2})^{\frac{1}{2}} = \exp(-t/T_g)$$

and

$$(\overline{s_d^2})^{\frac{1}{2}} \Big/ (\overline{s_o^2})^{\frac{1}{2}} = \exp(-t/T_d)$$

[1]

$(\overline{s_g^2})^{\frac{1}{2}}$ and $(\overline{s_d^2})^{\frac{1}{2}}$ are the root-mean-square slopes at time t during, respectively, the growth and the decay stage; $(\overline{s_o^2})^{\frac{1}{2}}$ is the steady state root-mean-square slope; T_g and T_d are the respective relaxation times for the growth and the decay of the mean-square slope. The fitted exponential curves are shown as the heavy lines in Figures 6 and 7. The data are seen in both figures to follow reasonably closely the fitted curves. The scatter of the data can not be avoided here, as the interval between data points is only one second.

5.2 Effects of Pre-Existing Waves on Growth and Decay of Ripples

The relaxation times for the growth and the decay of ripples over long pre-existing waves were obtained from Figures 6 and 7, and are tabulated in Table 2. The same times scales without pre-existing waves were reported earlier (Wu 1973c), and their values for the corresponding wind-shear velocities are also shown in Table 2.

HYDRONAUTICS, Incorporated

TABLE 2

Relaxation Time Scales of Growth and Decay of
Ripples With and Without Pre-Existing Waves

Wind Velocity U (m/s)	Growth Time, T_g (sec)		Decay Time, T_d (sec)	
	With	Without	With	Without
	Pre-Existing Waves			
4.18	2.13	7.7	93.4	28
6.92	2.32	4.2	69.0	25
9.60	3.13	0.9	44.6	17
12.25	4.17	0.1	50.3	18

A time lag between the sudden start of the wind and the exponential growth of root-mean-square surface slopes was observed earlier (Wu 1973c) in the present tank without pre-existing waves. Such a time lag is not seen in Figure 6. The growth time T_g shown in Table 2 for the case without pre-existing waves is that obtained from the earlier study with the time for wind initiation delayed by the time lag.

The growth times with pre-existing waves are seen in Table 2 to be shorter than those without at low wind velocities, and longer than those without at high wind velocities. Inasmuch as the shear velocities are the same for both cases, the difference is therefore merely due to the change of surface wave structures. The shortened growth time in the surface-tension governing regime with

parasitic capillaries may be due to the fact that a certain time is required for the carrier waves to develop from an initially calm water surface while the carrier waves already exist in the present experiment. The lengthened growth time in the gravity governing regime may be explained in the similar fashion as in the previous section regarding the effects of pre-existing waves on the mean-square slopes. The results at high wind velocities may be applicable to the oceanic condition, while the condition for the low wind velocities may exist only in laboratory wind-wave tanks (Wu 1970).

The decay times with pre-existing waves are seen in Table 2 to be much longer than those without for all wind velocities. This is apparently due to the slow damping of long carrier waves, and very active wave-wave interaction with ripples deriving energy from long carrier waves.

5.3 Differential Roughening and Smoothing of Wavy Surfaces

The growth and decay times for various segments of the carrier-wave profiles were obtained as discussed previously and are tabulated in Table 3. The general trends of the results are:

(1) There is no systematic indication of differential roughening of the windward and the leeward faces in either surface tension or gravity governing regime of wind-wave interaction.

(2) At the lowest wind velocity, the growth time is the longest for the upper half of leeward face, where parasitic capillaries are concentrated.

At the highest wind velocity, the growth is again the longest for the same segment of the wave profile, where violent wave breaking takes place. These trends are also true for the other wind velocities.

TABLE 3

Relaxation Times for Ripples Riding on Various
Portions of Carrier-Wave Profiles

Relaxation Time (sec)		Growth Time, T_g				Decay Time, T_d			
Wind Velocity, U(m/s)		4.18	6.92	9.60	12.25	4.18	6.92	9.60	12.25
Portion of Carrier Wave Profile	Entire Profile	2.13	2.32	3.13	4.17	93.4	69.0	44.6	50.5
	Leeward Face	3.14	2.09	3.09	4.19	94.5	74.4	42.2	41.5
	Windward Face	1.33	3.21	3.24	4.12	57.4	57.5	47.4	58.6
	Upper Half Leeward Face	4.02	2.12	3.31	7.34	125.5	48.7	32.6	19.5
	Lower Half Leeward Face	1.12	1.18	1.12	2.22	82.7	86.5	48.6	97.5
	Upper Half Windward Face	2.22	4.15	3.42	3.14	53.3	56.5	47.0	22.7
	Lower Half Windward Face	1.92	2.62	2.12	4.52	87.0	88.0	96.0	62.7

(3) The lower half of the leeward face is seen to provide the fastest response of the wind excitation.

(4) Opposite trends are seen at low and high wind velocities for the differential smoothing of the leeward and the windward faces. However, it is not clear why this is the case.

(5) The lower half of the windward face appears to have the fastest decay of ripple energy.

6. CONCLUDING REMARKS

The results obtained from the present experimental studies are summarized below:

(1) Effects of Pre-Existing Waves on Wind Boundary Layer and Microstructure: The effects of long pre-existing waves on the structures of wind and ripples are consistent. Compared on the basis of the wind-shear velocity, the roughness length of the wind boundary layer and the mean-square slope of the water surface are smaller with pre-existing waves than without. The reduction of mean-square slope by long carrier waves appear to provide a probable explanation of why the laboratory determined values are larger than oceanic ones, again compared on the basis of the wind-shear velocity.

(2) Correlation of Micro- and Macrostructures: The slope distributions of ripples on various segments of the carrier-wave profiles are skewed. In the surface-tension governing regime of wind-wave interaction, the leeward face is much rougher than the windward face. The parasitic capillaries are concentrated on the upper half of the leeward face at a lower wind velocity, and move further downward

HYDRONAUTICS, Incorporated

at higher wind velocities. In the gravity
governing regime, the difference in roughness
between the leeward and the windward faces becomes
smaller. However, the roughness on the windward
face is concentrated on the upper half of the wave
profile; the lower half of the windward face is the
smoothest segment of the long wave profile. These
observations may be helpful for setting the viewing
angle of the microwave sensors, and for interpreting
the results of the microwave measurements.

(3) Differential Roughening and Smoothing of Long
Surface Waves: Small differences in roughening
and smoothing of various segments of the carrier-
wave profile were found. An important finding in
this part of the study is that pre-existing waves
affect the growth and the decay time scales of
mean-square surface slopes, especially those at
high wind velocities. The wind and wave condi-
tions at high wind velocities are similar to oceanic
conditions. The relaxation time scales are found
to be much longer with than without the presence
of long carrier waves. The presence of long waves
eliminates wave components of intermediate lengths
and extracts the energy introduced by the wind
through ripples. These results are believed to be
important for studying wind-wave-current inter-
actions.

HYDRONAUTICS, Incorporated

REFERENCES

Cox, C. S. and Munk, W. H., 1956, "Slopes of the Sea Surface Deduced from Photographs of Sun Glitter," 6, No. 9, Scripps Institution of Oceanography.

Cox, C. S., 1958, "Measurements of Slopes of High-Frequency Wind Waves," J. Mar. Res. 16, 199-225.

Longuet-Higgins, M. S., 1963, "The Generation of Capillary Waves by Steep Gravity Waves," J. Fluid Mech. 16, 138-59.

Longuet-Higgins, M. S., 1969, "A Nonlinear Mechanism for the Generation of Sea Waves," Proc. Roy. Soc. A311, 371-89.

McGrath, J. R. and Osborne, M.F.M., 1973, "Some Problems Associated with Wind Drag and Infrared Images at Sea Surface," J. Phys. Oceangr. 3, 318-27.

Newton, R. W. and Rouse, J. W., Jr., 1972, "Experimental Measurements of 2.25-cm Backscatter from Sea Surfaces," IEEE Trans. GE-10, 2-7.

Phillips, O. M., 1963, "On the Attenuation of Long Gravity Waves by Short Breaking Waves," J. Fluid Mech. 16, 321-32.

Phillips, O. M., 1966, "The Dynamics of the Upper Ocean," Cambridge University Press.

Phillips, O. M., 1973a, "The Influences of Wind Drift and Capillarity on Blockage," HYDRONAUTICS, Incorporated Technical Report 7211-1.

Phillips, O. M., 1973b, "The Regeneration of Surface Waves by Wind in Interactions with Internal Gravity Waves (U)," HYDRONAUTICS, Incorporated Technical Report 7211-2, (CONFIDENTIAL).

Schlichting, H., 1968, "Boundary-Layer Theory," 6th Ed. McGraw-Hill Book Company, New York.

HYDRONAUTICS, Incorporated

Schooley, A. H., 1954, "A Simple Optical Method for Measuring
    the Statistical Distribution of Water Surface Slopes,"
    J Opt. Soc. Am., 44, 37-40.

Wu, Jin, 1968, "Laboratory Studies of Wind-Wave Interactions,"
    J. Fluid Mech. 34, 91-112.

Wu, Jin, 1970, "Wind-Wave Interactions," Phys. Fluids 13,
    1926-1930.

Wu, Jin, 1971a, "Slope and Curvature Distributions of Wind-
    Disturbed Water Surface," J. Opt. Soc. Am. 61, 852-58.

Wu, Jin, 1971b. "Observations on Long Waves Sweeping Through
    Short Waves," Tellus 23, 364-70.

Wu, Jin, 1972a, "Surface Curvature of Wind Waves Observed from
    Different Angles," J. Opt. Soc. Am. 62, 395-400.

Wu, Jin, 1972b, "Physical and Dynamical Scales for Generation of
    Wind Waves," J. Waterways, Harbor Coastal Engr. Div.
    ASCE 98, WW2, 163-175.

Wu, Jin, 1973a, "Effects of Wind-Induced Drift Currents on the
    Propagation of Surface Waves," HYDRONAUTICS, Incorporated
    Technical Report 7211-3.

Wu, Jin, 1973b, "Wind-Induced Drift Current," HYDRONAUTICS, In-
    corporated Technical Report 7303-3.

Wu, Jin, 1973c, "Rates of Growth and Decay of Wind Waves under
    Conditions of Unsteady Wind," HYDRONAUTICS, Incorporated
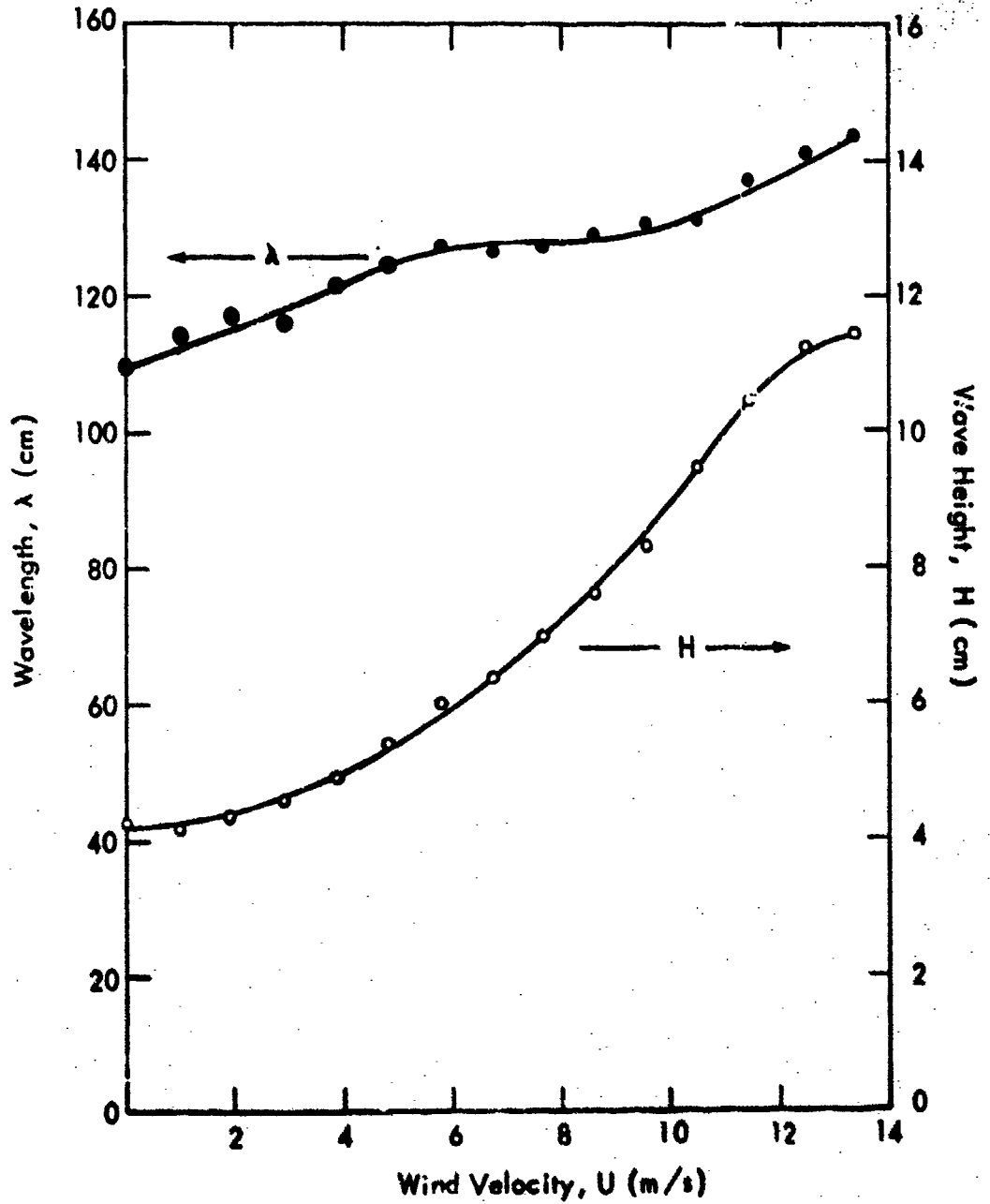   Technical Report 7211-4.

FIGURE 1 - AVERAGE WAVELENGTHS AND WAVE HEIGHTS UNDER
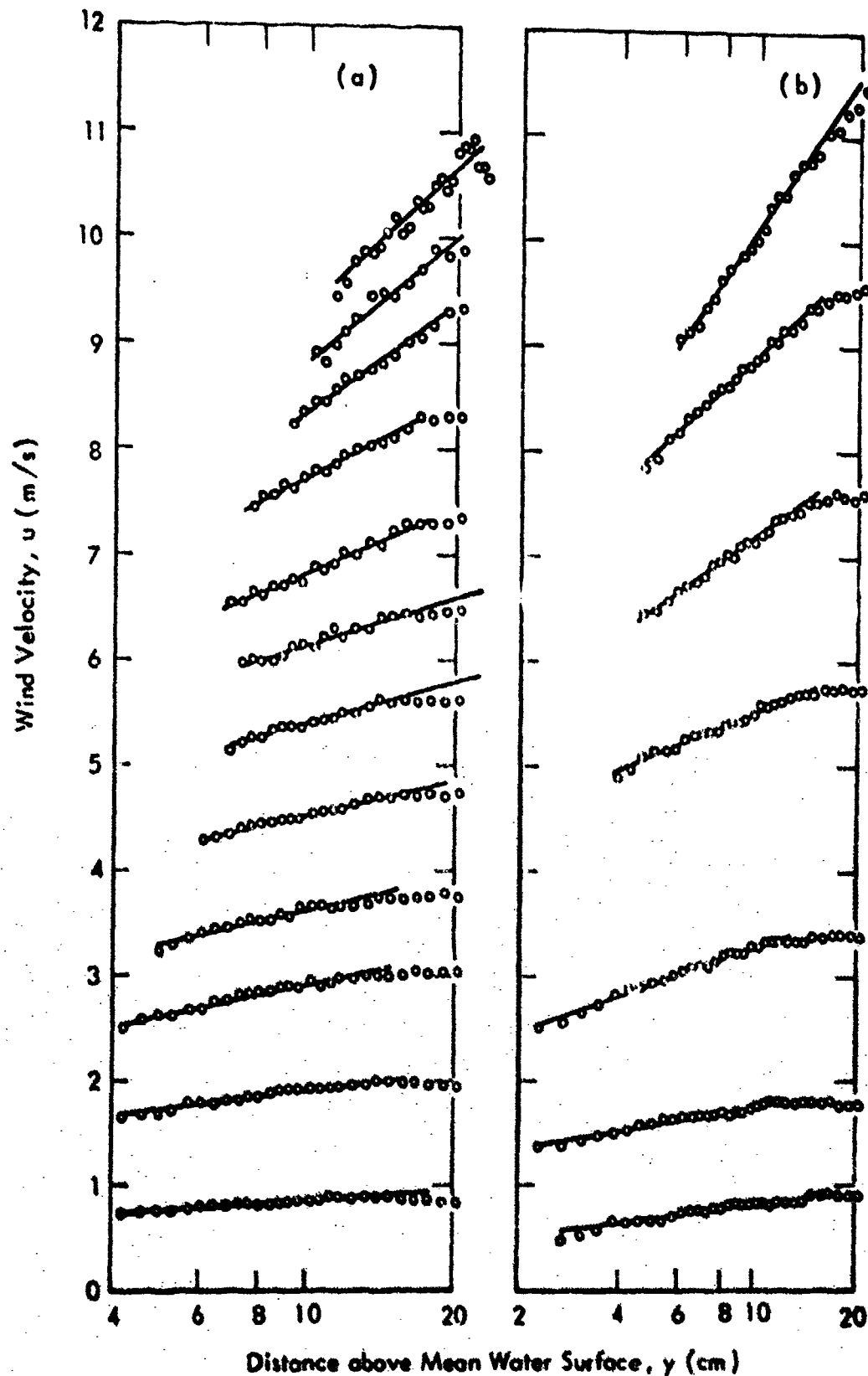VARIOUS WIND VELOCITIES

FIGURE 2 - VELOCITY DISTRIBUTIONS OF WIND BLOWING OVER PRE-EXISTING WAVES OF LARGE AMPLITUDE (a) AND OF SMALL AMPLITUDE (b). In each block the profiles were obtained from bottom to top at the order of increasing freestream wind velocities.
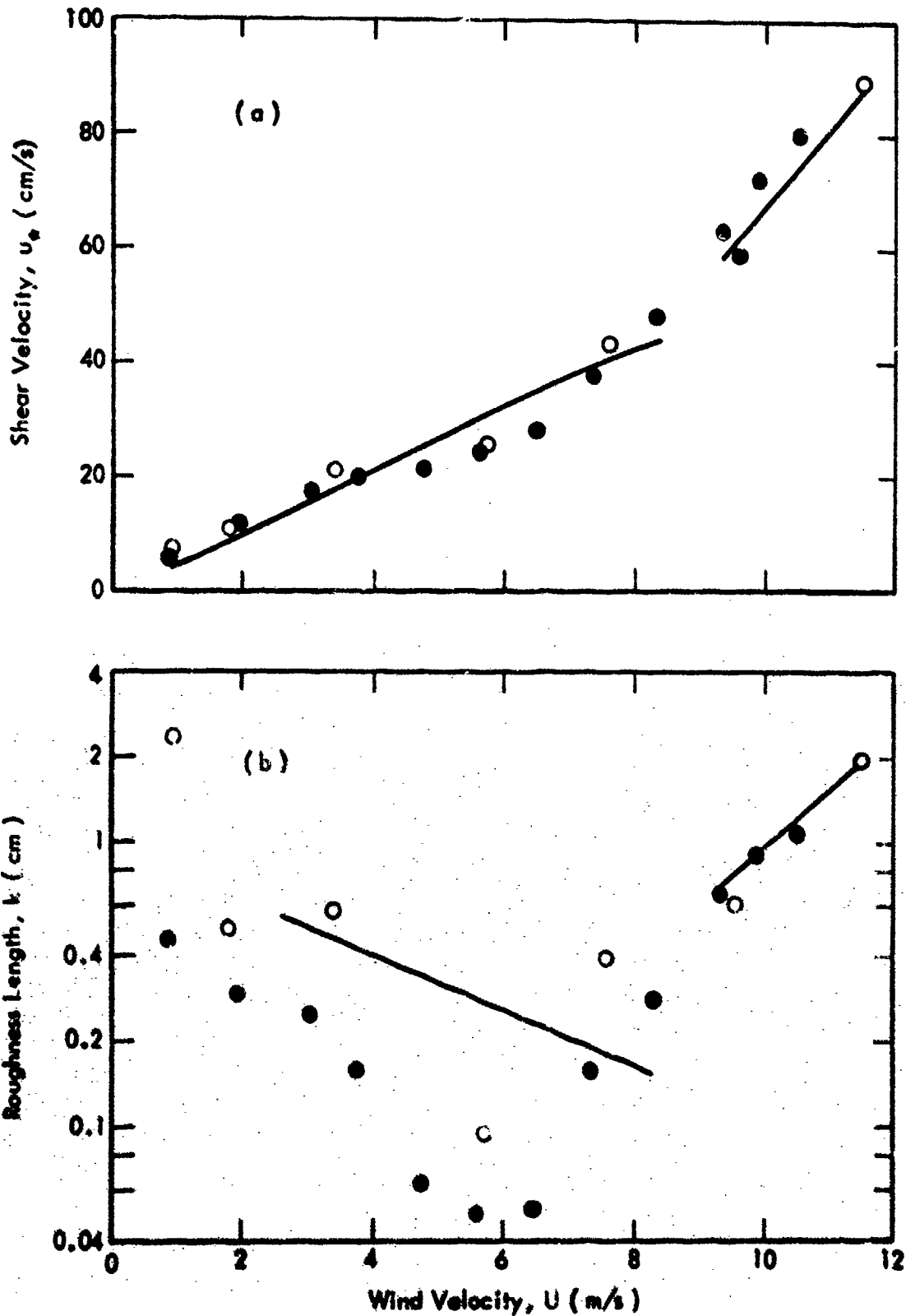
FIGURE 3 - SHEAR VELOCITIES AND ROUGHNESS LENGTH OF WIND
OVER PRE-EXISTING WAVES OF LARGE AMPLITUDE (●)
AND OF SMALL AMPLITUDES (O). The solid lines indicate
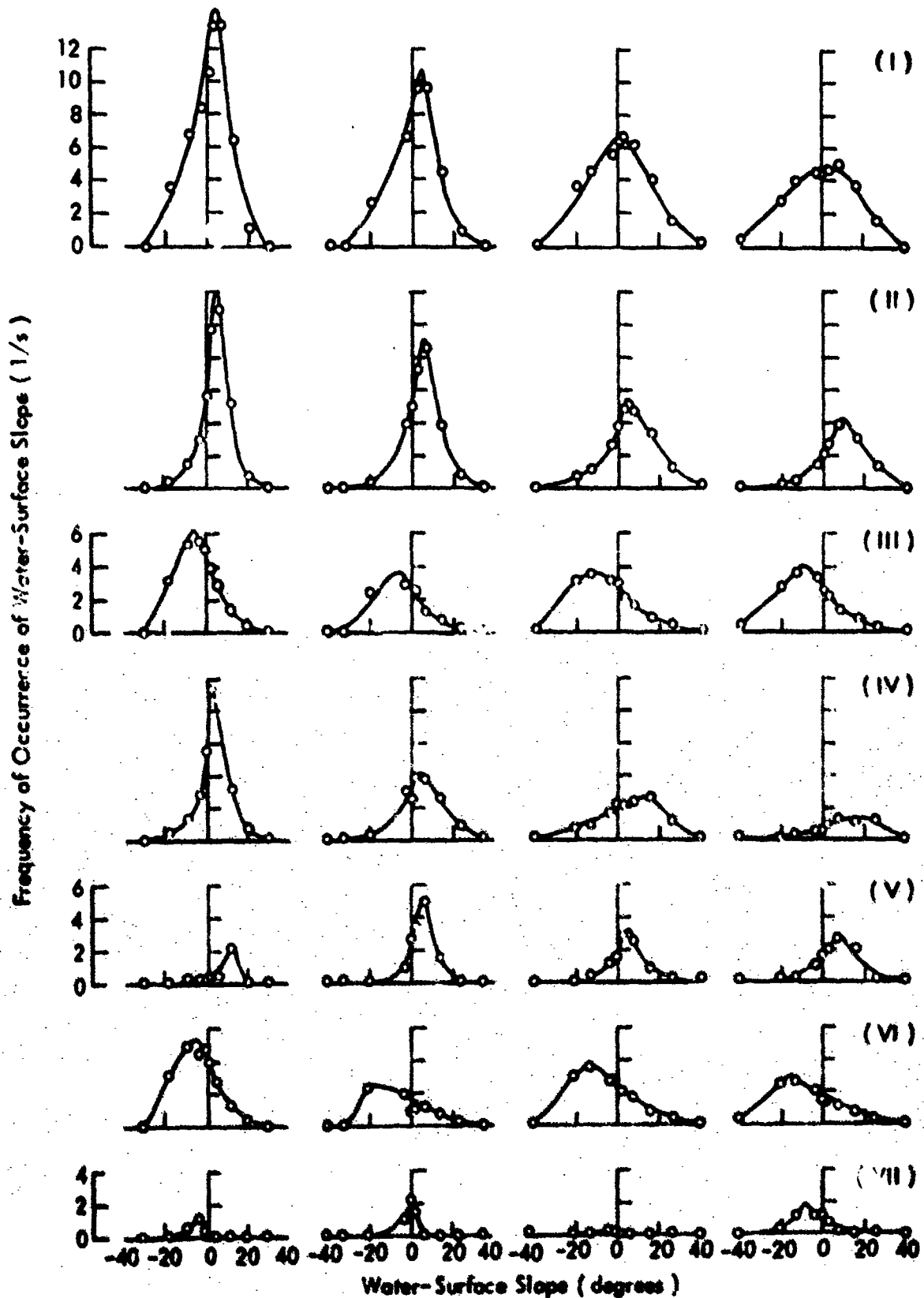the results obtained earlier (1973 b) without pre-existing
waves.

FIGURE 4 - SLOPE DISTRIBUTION OF RIPPLES RIDING ON VARIOUS PORTIONS
OF CARRIER-WAVE PROFILES. The data were obtained from the follow-
ing portions of the carrier-wave profile: (I) entire profile ,(II) leeward
face, (III) windward face, (IV) upper half of leeward face, (V)
lower half of leeward face, (VI) upper half of windward face, (VII)
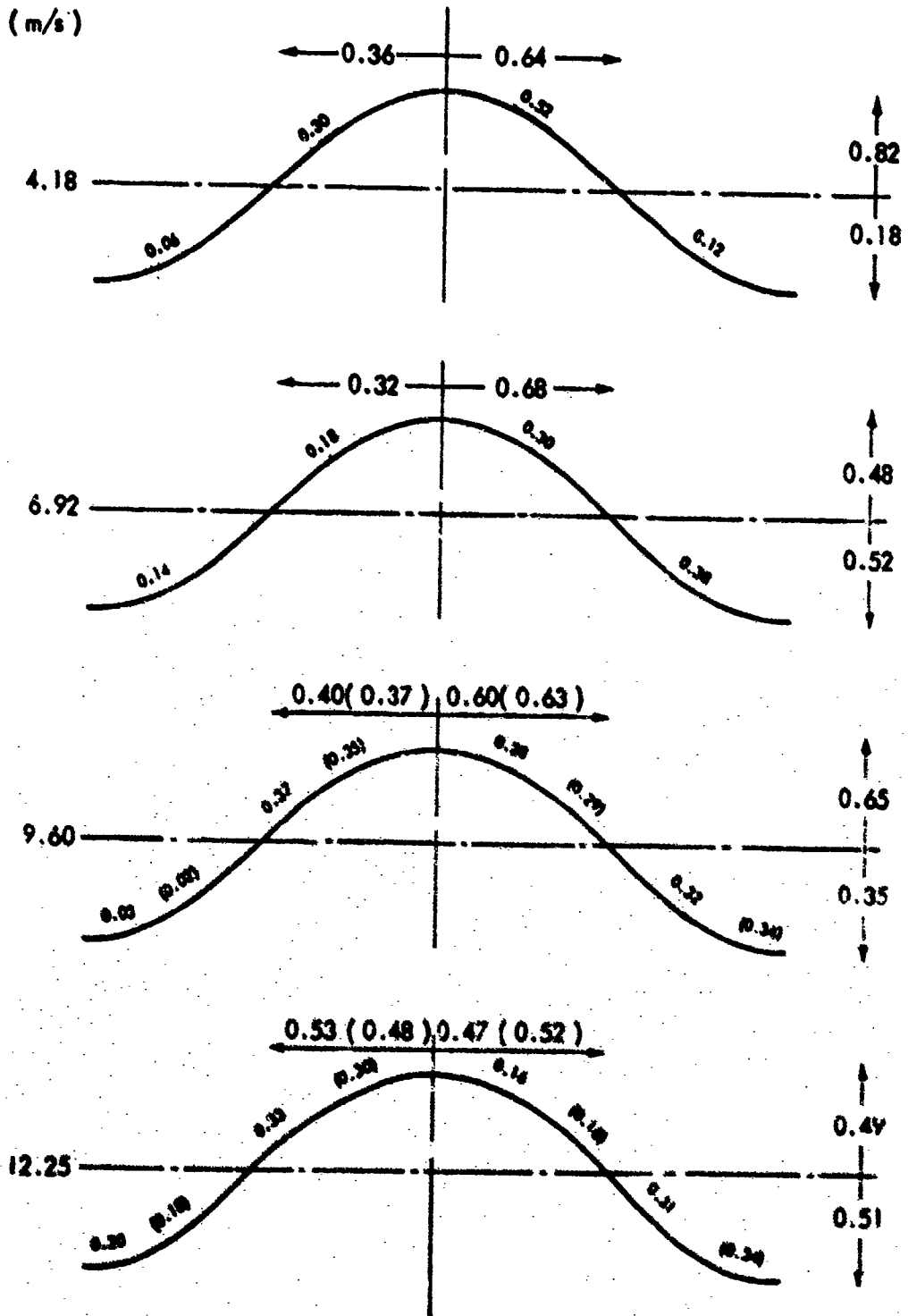lower half of windward face

HYDRONAUTICS, INCORPORATED

U (m/s)

FIGURE 5 – DISTRIBUTIONS OF RIPPLES ALONG CARRIER-WAVE
PROFILES. The wind direction is from left to right of
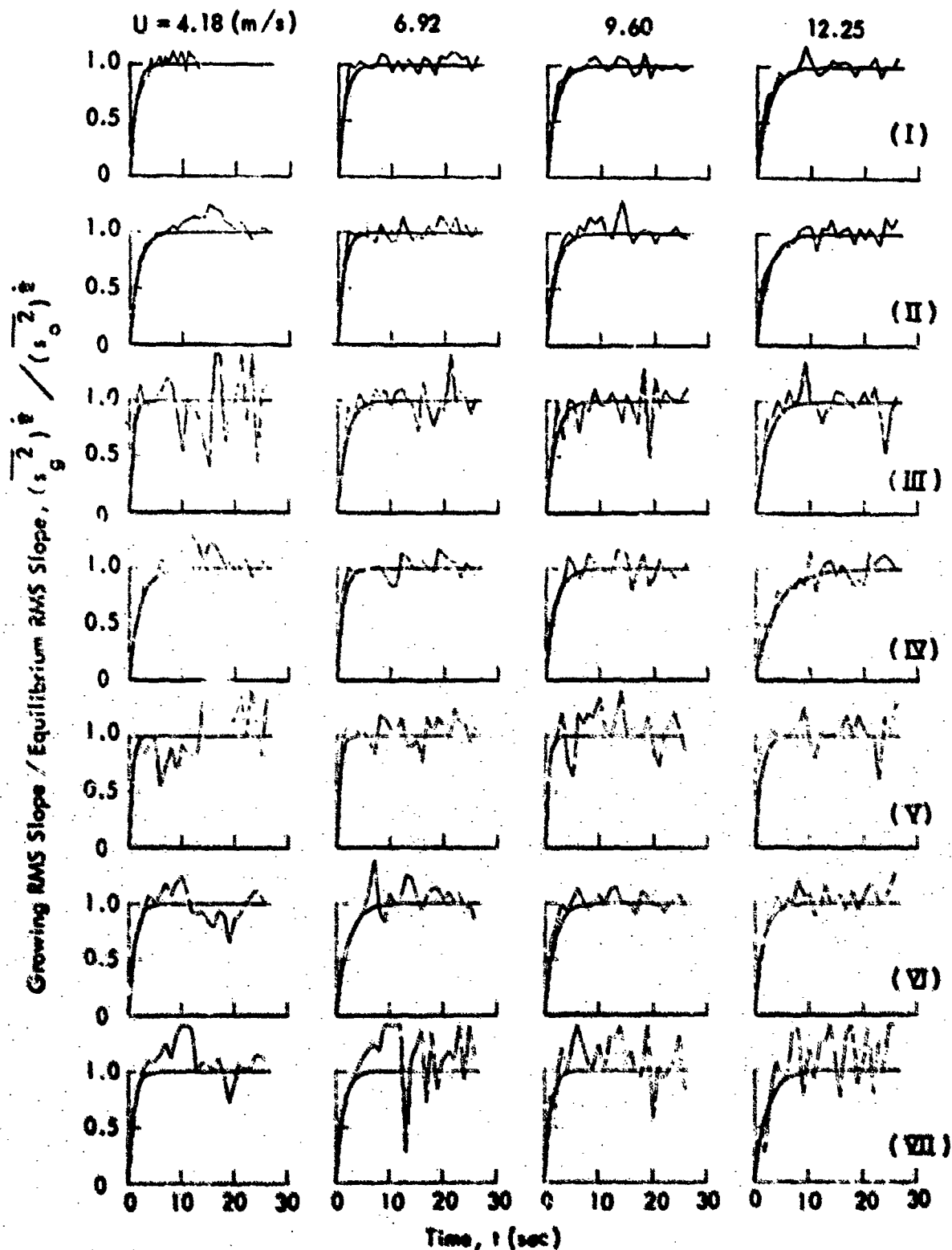the figure.

FIGURE 6 – EXPONENTIAL GROWTH OF ROOT-MEAN-SQUARE SLOPE FOLLOWING A SUDDEN WIND START. The row number shown on the right side of the figure is the same as that indicated in Figure 4.
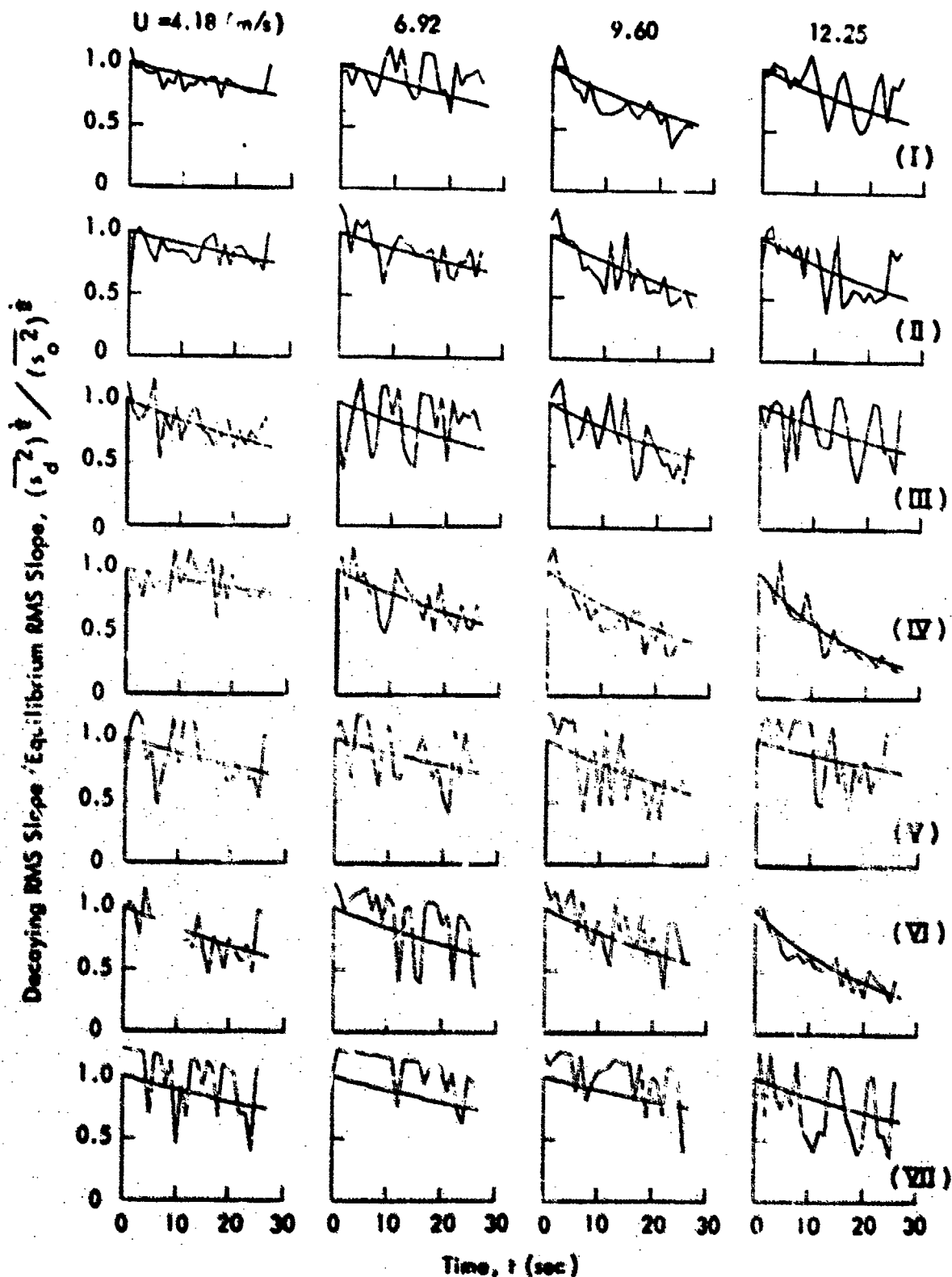
FIGURE 7 - EXPONENTIAL DECAY OF ROOT-MEAN-SQUARE SLOPE FOLLOWING A SUDDEN WIND STOPPAGE. The row number shown on the right side of the figure is the same as that indicated in Figure 4.

HYDRONAUTICS, Incorporated

DISTRIBUTION LIST
Contract No. N00014-72-C-0509
NR 062-472

Dr. J. D'Albora
Naval Underwater Systems Cen.
Newport, Rhode Island 02840   1

Johns Hopkins University
Applied Physics Laboratory
8621 Georgia Avenue
Silver Spring, Maryland 20910
Attn: L. Cronvich   1
       H. Gilreath   1
       A. Stone   1

University of California, SD
Marine Physical Laboratory
Scripps Inst. of Oceanography
San Diego, Calif. 92152
Attn: Dr. F. Spiess   1

Dr. Martin H. Bloom
Polytechnic Inst. of Brooklyn
Route 110
Farmingdale, N. Y. 11735   1

General Research Corporation
1501 Wilson Blvd., Suite 700
Arlington, Va. 22209
Attn: Mr. P. Donahoe   1

Dr. Marvin King
Riverside Research Inst.
80 West End Avenue
New York, New York 10023   1

Dr. James Young
Science Applications, Inc.
P.O. Box 2351
La Jolla, Calif. 92037   1

Mr. V. Lujetic
Tetra Tech, Inc.
1911 N. Ft Myer Drive
Arlington, Virginia 22209   1

University of California
Lawrence Livermore Laboratory
P. O. Box 808
Livermore, Calif. 94550
Attn: Dr. H. P. Smith   1
       Dr. Michael Wirth   1

Dr. W. S. Lewellen
Aeronautical Res. Associates
  of Princeton, Inc.
50 Washington Road
Princeton, New Jersey 08540   1

R&D Associates
P. O. Box 3580
Santa Monica, Calif. 90403
Attn: Dr. D. Holliday   1
       Dr. F. L. Fernandez   1
       Dr. M. Milder   1

Dr. K. V. Saunders
Pacific-Sierra Research Corp.
P. O. Box 578
Malibu, California 90625   1

Dr. Thomas Taylor
The Aerospace Corporation
P. O. Box 92957
Los Angeles, Calif. 90009   1

TRW Systems Group
One Space Park
Redondo Beach, Calif. 90278
Attn: J. Chang   1
       E. Baum   1

HYDRONAUTICS, Incorporated

-2-

Mr. L. W. Griswold
Naval Ship Research &
  Development Center
Annapolis Laboratory
Annapolis, Md. 21402   1

Dr. Frank Lane
KLD Associates, Inc.
7 High Street, Suite 204
Huntington, New York 11743   1

Dr. M. Y. H. Pao
Flow Research, Inc.
1819 S. Central Ave., Suite 72
Kent, Washington 98031   1

Dr. D. R. S. Ko
Flow Research, Inc.
5959 West Century Blvd.
Los Angeles, Calif. 90045   1

HYDRONAUTICS, Incorporated
Pindell School Road
Howard County
Laurel, Maryland 20810
Attn: Dr. J. Wu   1
       Dr. T. R. Sundaram 1

Xonics, Inc.
6837 Hayvenhurst Ave.
Van Nuys, California 91406
Attn: Dr. M. Balser   1

Dr. J. Alex Thomson
Physical Dynamics, Inc.
P. O. Box 1069
Berkeley, California 94701   1

Dr. Roberto Vaglio-Laurin
Advanced Technology Labs., Inc.
400 Jericho Turnpike
Jericho, New York 11753   1

Mr. R. Rehm
CALSPAN Corporation
P. O. Box 235
Buffalo, New York 14221   1

Stanford Research Institute
333 Ravenswood Avenue
Menlo Park, California 94025
Attn: H. Guthardt   1
      K. Krishnan   1

Institute for Defense Analyses
400 Army Navy Drive
Arlington, Virginia 22202
Attn: Dr. P. A. Selwyn 1
      Dr. Joel Bengston 1
      Mr. J. C. Nolen 1

Naval Research Laboratory
4555 Overlook Avenue
Washington, D. C. 20390
Attn: F. MacDonald   1
      J. O. Elliot   1
      K. G. Williams 1
      S. Piacsek   1
      A. H. Schooley 1

Office of Naval Research
800 N. Quincy Street
Arlington, Virginia 22217
Attn: M. Cooper (438) 1
      R. Cooper (438) 1
      J. Witting (481) 1
      Cdr. J. Ballou (466) 1
      Dr. S. Reed (102T) 1

Naval Undersea Center
San Diego, California 92132
Attn: O. Lee   1
      K. Nelson   1

Defense Advanced Research Projects Agency 1400 Wilson Blvd. Arlington, Virginia 22209		Naval Scientific & Technical Intelligence Center 4301 Suitland Road Washington, D. C. 20390
Attn: K. Kresa, TTO	1	Attn: Capt. J. P. Prisley 1
S. Ruby, MATS	1	
R. Hoglund, STO	1	Mr. I. H. Gatzke Naval Air Systems Command Department of the Navy
ODDR&E The Pentagon Washington, D. C. 20301		Washington, D. C. 20360 1
Attn: D. R. Heebner, 3E1040	1	Defense Documentation Center
N. F. Wikner, 3E1087	1	Cameron Station
G. Cann, 3D1048	1	Alexandria, Virginia 22314 12

Director
Central Intelligence Agency
Main Station
Washington, D. C. 20305
Attn: H. Farmer   1

Cdr. D. Walsh
OASN/R&D
The Pentagon, 4E471
Washington, D. C. 20350   1

Mr. D. A. Rogers
SP 2018/NSP
Department of the Navy
Washington, D. C. 20390   1

Cdr. R. Miller
Ofc Chief of Naval Operations
The Pentagon, 5D572
Washington, D. C. 20350   1

Captain D. Keech
Deputy Director of Navy Labs
Department of the Navy
Washington, D. C. 20360   1